An Interdisciplinary View of Interfaces: Perspectives Regarding Emergent Phase Formation

Kyle S. Brinkman[1]
Department of Materials Science
and Engineering,
Clemson University,
Clemson, SC 29634
e-mail: ksbrink@clemson.edu

A perspective on emergent phase formation is presented using an interdisciplinary approach gained by working at the "interface" between diverse application areas, including solid oxide fuel cells (SOFCs) and ionic membrane systems, solid state lithium batteries, and ceramics for nuclear waste immobilization. The grain boundary interfacial characteristics of model single-phase materials in these application areas, including (i) CeO_2, (ii) $Li_7La_3Zr_2O_{12}$ (LLZO), and (iii) hollandite of the form $Ba_xCs_yGa_{2x+y}Ti_{8-2x-y}O_{16}$, as well as the potential for emergent phase formation in composite systems, are discussed. The potential physical properties resulting from emergent phase structure and distribution are discussed, including an overview of existing three-dimensional (3D) imaging techniques recently used for characterization. Finally, an approach for thermodynamic characterization of emergent phases based on melt solution calorimetry is outlined, which may be used to predict the energy landscape including phase formation and stability of complex multiphase systems. [DOI: 10.1115/1.4037583]

Introduction

It is well known that the interfaces such as grain boundaries and surfaces play a large role in determining overall materials properties. It is also known that the composition and structure of interfaces is inherently different from bulk materials. For instance, aliovalent dopants, used to tune the bulk point defect concentrations, are known to accumulate at interfaces resulting in spatially varying defect concentrations and potential barriers for charge transport [1]. One solution to this issue has been to target single crystalline or high quality epitaxial films with negligible grain boundary area [2,3].

However, polycrystalline materials are low cost, easy to process, and remain the materials form of choice for a majority of energy conversion systems such as fuel cells and batteries. These materials are typically designed to limit phase interactions between the functional materials of the device. For instance, at solid oxide fuel cell operating temperature, chromium (Cr) vapor species may evaporate over chromia-forming alloy interconnects and redeposit as oxide scales resulting in a reduction in oxygen reduction activity and degradation of the fuel cell performance [4,5]. Despite efforts to limit reactions, there are many examples of emergent phase formation in materials systems occurring during operation or fabrication. This work explores an alternative approach; instead of avoiding phase interactions, how can their formation be understood, controlled, and ultimately utilized as a tool to tune the materials properties?

This perspective article addresses this question using an interdisciplinary approach gained by working at the "interface" between disciplines and applications. A surprising fact in industry specific research topics is that diverse fields such as nuclear energy (including nuclear fuel and waste immobilization materials) and renewable energy areas, including solid oxide fuel cell and Li-ion battery systems, utilize many of the same classes of materials. For instance, fluorite structures such as CeO_2, ZrO_2,

and derivatives possess high levels of oxygen ion conductivity for use as solid oxide fuel cell electrolytes [6]. In addition, CeO_2 is a well-known surrogate for UO_2, and the principal actinide components of nuclear fuel UO_2 and PuO_2 also crystallize in fluorite structured oxides [7]. Garnet structures currently being evaluated for solid-state lithium battery electrolytes such as $Li_7La_3Zr_2O_{12}$ (LLZO) are similar to based garnets being evaluated for nuclear waste immobilization of lanthanide fission products [8,9]. Finally, tunnel structured materials such as hollandites which incorporate mobile alkali ions such as Li, K, and Na in tunnels have been looked at as candidate battery electrode materials [10]; current work in solid state materials synthesis in the nuclear materials realm seeks to engineer the tunnels to block the motion of larger alkali ions such as Cs for immobilization applications [11]. These examples highlight the importance of an interdisciplinary approach; learning how researchers in one application area "promote" transport, may be used in other disciplines interested in "blocking" transport.

Figure 1 illustrates the concept of "emergent" phase formation arising during the processing operation of binary phase mixtures. Mixtures or composites are frequently used to tune the materials properties. For instance, in fuel cell and ionic membrane applications, separate ionic and electronic conductive phases offer a flexible way to tune the conductivity by varying the volume fraction of constituent phases. Secondary phase formation or emergent phases can occur in the bulk of the material (three-dimensional (3D)) or can form at distinct interfaces (two-dimensional) such as the electrolyte/electrode boundary. This article compares emergent phase formation in three application areas: (a) solid oxide fuel cells and ionic membrane systems, (b) solid state lithium batteries, and (c) ceramics for nuclear waste immobilization. The initial discussion focuses on the grain boundary interfacial characteristics of model single-phase materials in these application areas, including (i) CeO_2, (ii) $Li_7La_3Zr_2O_{12}$ (LLZO), and (iii) hollandite of the form $Ba_xCs_yGa_{2x+y}Ti_{8-2x-y}O_{16}$, followed a discussion of emergent phase formation encountered when these are used in materials systems for their respective applications. Next, a review of imaging techniques that are currently employed to
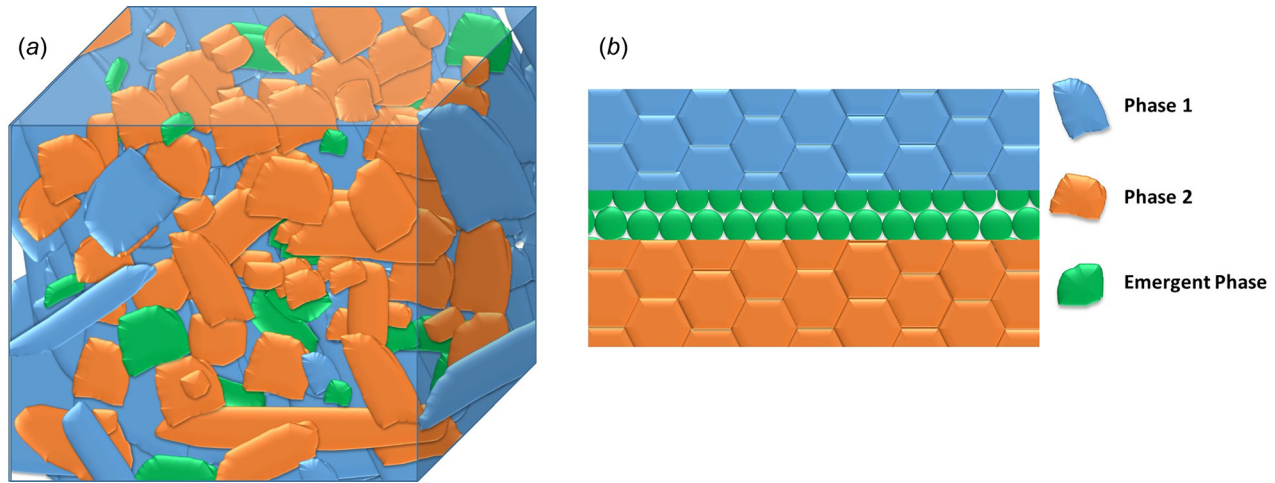

Fig. 1 (*a*) Emergent phase distributed in 3D bulk of the material for and (*b*) two-dimensional model for electrode and electrolyte interfacial layer formation

examine the 3D distribution of emergent phases is presented. Finally, an approach for thermodynamic characterization of emergent phases based on melt solution calorimetry is outlined which may be used to predict the energy landscape, including phase formation and stability of complex multiphase systems.

Model Single Phase Materials: Interfacial Characteristics

Oxygen Ion Conducting System CeO_{2-x}. *Exactly what is the structure and mechanisms responsible for interfaces which facilitate or inhibit ionic transport?* The common lexicon in solid state ionics is to refer to "grain boundaries" as one type of material with the same characteristics. However, researchers in structural ceramics have explored grain boundary phase formation and local structure in alumina based materials as they seek to understand grain growth and failure mechanisms [12,13]. A recent work has shown that grain boundaries may be disordered or may be interface stabilized phases that are chemically and structurally distinct from any bulk phase [14].

In the oxygen ion conducting system CeO_2 model, nanocrystalline cerium oxide was shown to have orders of magnitude enhanced electronic conductivity as compared to micron sized grain materials [1,15,16]. This enhanced electronic conductivity has been attributed to (i) the reduced enthalpy of reduction at the grain boundaries resulting from the large interfacial area to volume ratio in nanocrystalline specimens, combined with (ii) space charge effects resulting from grain/grain boundary surface contact where electron concentration is enhanced in the grain boundaries while positively charged oxygen vacancies are depleted. Ionic solids are overall neutrally charged, but there are local areas of electrostatic charge commonly known as space charge regions. In ceria systems, a depletion of oxygen vacancies and enhancement of electrons are predicted and experimentally observed leading to a decrease in oxygen ion conductivity and increase in electronic conductivity with decreasing grain size. Figure 2(*a*) shows space charge profiles of acceptor dopants, oxygen vacancies, and electrons near a grain boundary interface in CeO_2 with a space charge potential of +0.4 V, according to two different boundary conditions (Gouy–Chapman solid line and Mott Schottky dotted line) [17]. The resulting grain size dependent ionic and electronic conductivity values for this system are presented in Fig. 2(*b*), and ambipolar dependent oxygen flux for nanocrystalline CeO_2 is shown in Fig. 2(*c*). It is noted that Fig. 2 presents the case of pure or slightly doped systems (less than 0.1% or 1000 ppm) where space charge can extend to several tens of nanometers from the grain boundary interface. In highly doped systems (1–10% levels), the space charge region may extend only a few nanometers from the interface [16,18]. The size effects depicted in Fig. 2 arise from altered defect concentrations *and* distributions. These effects provide an alternative way to modify the material's defect structure without changing the ratio of the chemical constituents.
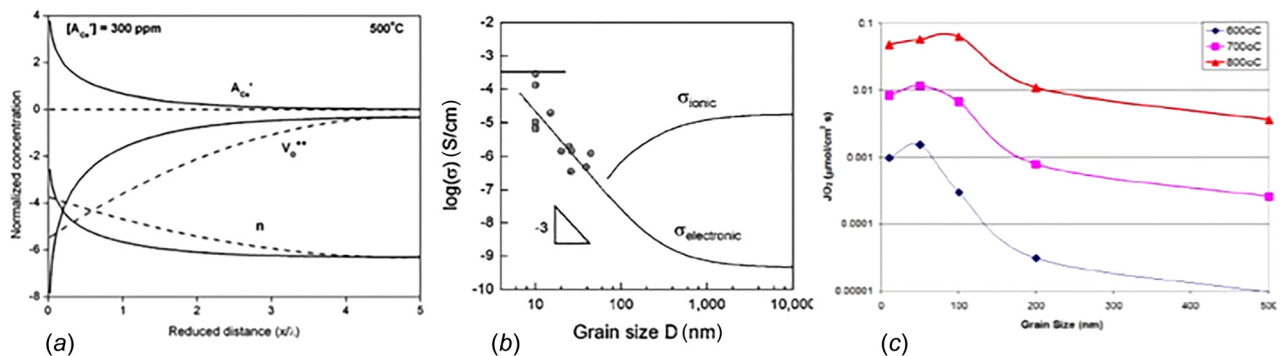

Fig. 2 (*a*) Space charge profiles of acceptor dopants, oxygen vacancies, and electrons near a grain boundary interface in CeO_2[17], (*b*) ionic and electronic conductivity dependence on grain size at 500 °C in air for CeO_2[17]. (Reproduced with permission from Tuller et al. [17]. Copyright 2009 by the PCCP Owner Societies), and (*c*) oxygen flux μmol/cm^2 s versus grain size and temperature for CeO_2 nanocrystalline membranes [19]. (Reproduced with permission from Brinkman et al. [19]. Copyright 2010 by Journal of The Electrochemical Society.)
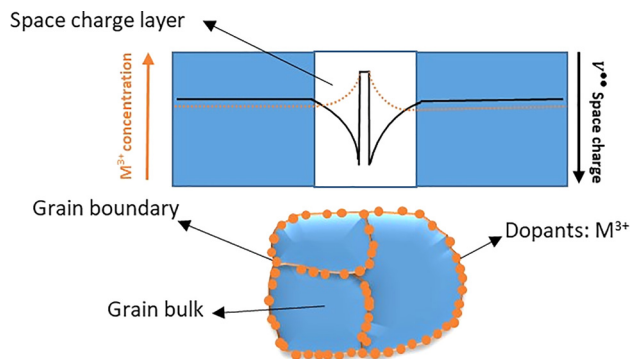
Fig. 3 M^{+3} dopant distribution at grain boundaries resulting in the formation of an interfacial space charger layer

Accompanying the changes in local composition at the interface is volumetric expansion or contraction referred to as chemical expansion [20]. For example, in the CeO_2 materials presented in Fig. 1, reducing conditions leading to enhanced oxygen vacancies result in linear volume expansion attributed to the larger Ce^{+3} reduced state ion as compared to Ce^{+4} over the range $x = 0$–0.2 [21]. Alternatively, if changes in chemical composition may induce strain, then it might be supposed that strain may impact local composition and be used to control transport. Theoretical predictions for the CeO_2 system indicated that compressively strained ceria exhibited increased activation energy for oxygen vacancy migration as compared to tensile strained materials [22,23]. Quantitatively, they predicted an increase in the conductivity by 4 orders of magnitude with a 4% level of biaxial tensile strain. This type of strain is typically encountered in thin films specimens constrained by a substrate. Experimental works have verified the impact of strain on the ionic conductivity of ceria and zirconia based thin films [24,25].

Of particular interest for the consideration of electronic properties is the well-known propensity for dopants to preferentially segregate at grain boundaries leading to changes in local defect concentrations [26]. High resolution scanning transmission electron microscopy has revealed evidence of Gd segregation in both the bulk as nanodomains as well as at the grain boundaries [27–30]. Figure 3 graphically illustrates the aggregation of M^{+3} dopants substituted on M^{+4} sites at the grain boundary resulting in decreased oxygen vacancy concentration at the interface. Dopant segregation at the interface also represents a local driving force for emergent phase formation [31].

Solid State Lithium Ion Conductors $Li_7La_3Zr_2O_{12}$. Garnet-type $Li_7La_3Zr_2O_{12}$ (LLZO) has been demonstrated as a promising solid-state electrolyte material for lithium ion batteries. Solid state electrolytes with room temperature conductivities in excess of 10^{-4} S/cm are being considered as a substitute for the current liquid electrolyte and polymer based separators which would result in the enhanced safety. Weppner and coworkers reported a group of garnet-type fast lithium ionic conductors with the chemical formula of $Li_5La_3M_2O_{12}$ (M = Nb, Ta) 2003 which exhibited appreciable bulk ionic conductivity $\sim 10^{-6}$ S/cm at 25 °C [32]. Studies on the structure of LLZO strongly indicated that the inclusion of dopants such as aluminum ions (Al^{3+}) helps to stabilize the cubic symmetry at high temperature. More recently, Murugan et al. reported $Li_7La_3Zr_2O_{12}$ (LLZO) with bulk lithium ionic conductivity of 10^{-4} S/cm at 25 °C [33]. However, lithium loss due to high temperatures employed during sintering led to the formation of a pyrochlore phase $La_2Zr_2O_7$ which impedes Li transport [34,35].

The addition of select dopants was found to decrease pyrochlore phase formation and also demonstrated an impact on the symmetry of the primary crystalline phase. Cubic and tetragonal LLZO were identified by Awaka et al. [36,37]. In general, lithium ion conductivity of the cubic phase LLZO is higher than that of tetragonal LLZO by 2 orders of magnitude. However, the details of the phase transition between these two phases are not completely understood. Multiple doping strategies have been investigated in order to prevent secondary phase formation and to stabilize the cubic structure of LLZO at room temperature; candidates include aluminum (Al) [38–42], yttrium (Y) [43], gallium (Ga) [39,44–46], tantalum (Ta) [39,47], niobium (Nb) [48], and tungsten (W) [49]. Recent studies focused on controlling the grain boundary area by spark plasma sintering in conjunction with high temperature annealing indicated when multiple effects were taken into consideration, samples with a larger grain size exhibited higher total lithium conductivity pointing to blocking role of the interface on ionic transport [46].

Cs Containing Hollandite $Ba_xCs_yGa_{2x+y}Ti_{8-2x-y}O_{16}$. One-dimensional tunnel structures have been widely studied for their potential as fast-ionic conductors due to the high mobility of A-site cations in tunnels [10,50]. One class of these materials are termed Hollandites, which are in the priderite minerals group with a general formula of $(K,Ba)(Ti,Fe)_8O_{16}$, in which the majority of the M-site is replaced with Ti. Hollandite-type structures can exist in both tetragonal ($I4/m$) and monoclinic ($I2/m$) phases, exhibiting tunnels formed by linked oxygen octahedra. The size and geometry of these tunnels serve to facilitate or impede the mobile alkali and alkaline-earth ions that reside on the A-site in these tunnels [11,51]. The polycrystalline hollandites were originally investigated as sodium and potassium ion conductors exhibiting ion conductivity on the order of magnitude of 10^{-4} (S/cm) at 300 °C. Later studies evaluated lithium ion insertion into hollandites with multivalent M site dopants such as Fe, Mn for use as cathode materials in lithium ion batteries [52].

Hollandite structures, similar to those used in the battery work, have also demonstrated the ability to incorporate larger cations in tunnel sites such as cesium which is one of the more problematic radionuclides to immobilize because of its volatility at high temperature and its tendency to form water-soluble compounds [53]. By selective choice of dopants, the tunnels that allow lithium, sodium, and potassium mobility can be tuned to form a bottle-neck, which acts to impede Cs which occupies the available tunnel sites. Early studies of hollandite focused on phase formation with several B-site cations (e.g., Al, Ti, and Fe) but limited Cs-incorporation ($\sim$1.3 wt %) [54,55]. More recent work has demonstrated the stability of high Cs containing compositions. Structural studies demonstrated the higher Cs loading resulting in a framework expansion in the direction perpendicular to the tunnel axis due to the incorporation of the larger Cs ions, resulting in less distortion in the oxygen octahedra and a more symmetric structure [11,56]. Higher symmetry structures resulted in a more stable hollandite in terms of formation enthalpy with respect to their constituent oxides. Despite increased oxygen to oxygen distance in the tunnel, the values were still small enough to trap the Cs, which is essential for applications as a nuclear waste form.

In addition to atomic features such as tunnel size, microstructural features were shown to affect ion mobility. High Cs-content compositions revealed large rod-like grains and the largest measured total conductivity by impedance methods. Using equivalent circuit modeling to separate bulk versus grain boundary effects in these materials indicated bulk conductivity was similar at high and low Cs loadings; while interfacial resistance was greatest at fine grained (low Cs compositions) [11]. The behavior of the atomistic level tunnel size and the microstructure dependence on cesium concentration is depicted in Fig. 4. Therefore, the grain boundary "blocking" effect is similar to findings in fields of oxygen ion conductors and solid-state lithium ion conductors.
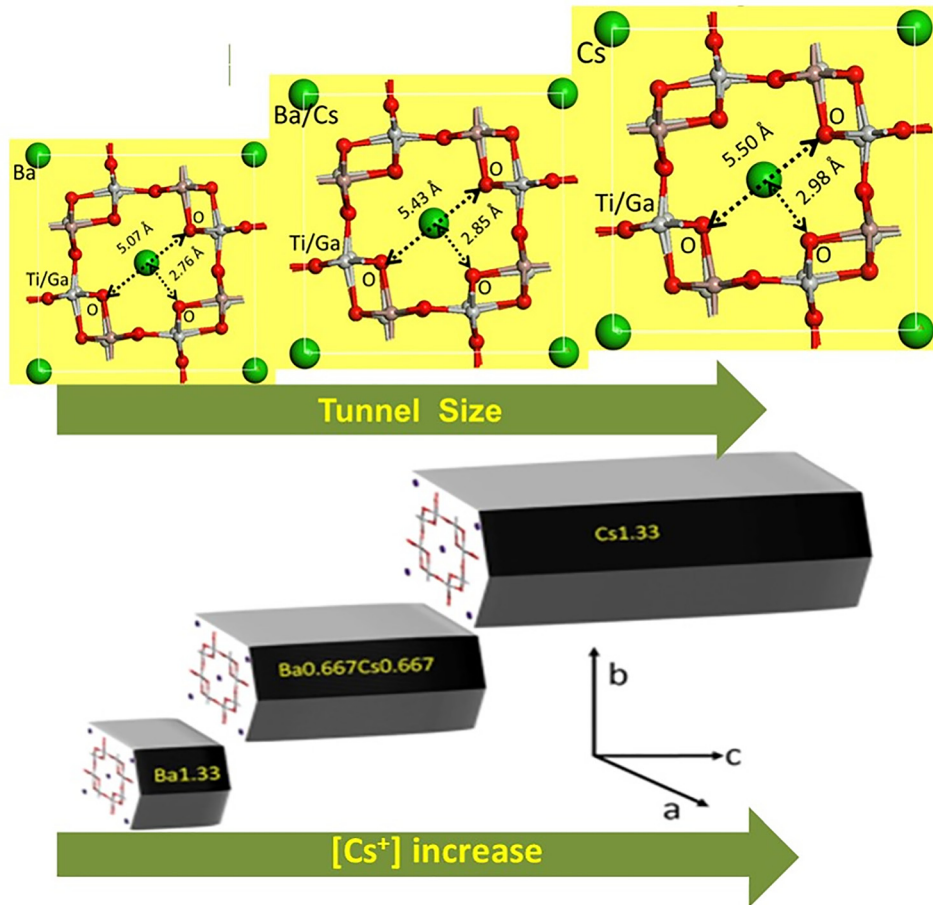
Fig. 4 Perspective view of hollandite structure along [001] tunnel direction and graphic depicting microstructure as a function of Cesium concentration. (Reproduced with permission from Xu et al. [11]. Copyright 2016 by Scientific Reports.)

Model Multiphase Heterogeneous Systems: Emergent Phase Formation

Dual Phase Ionic and Electronic Conductive Systems. Dual phase mixed ionic and electronic conductive (MIEC) materials systems consisting of separate ionic and electronic conductive phases offer an alternative solution to tune electrical and mechanical properties in energy conversion systems. Property tuning appears to be flexible and straightforward in dual-phase MIECs (DP-MIECs), as both the ionic conductors and the electronic conductors have been well developed [1,57,58]. However, the performance of DP-MIECs is not necessarily controlled by the properties of individual constituents. Phase interactions and altered interfaces such as grain boundaries play a role in determining the overall performance [31,59,60].

Recent work on the DP MIEC system $Ce_{0.8}Gd_{0.2}O_{2-\delta}$-$CoFe_2O_4$ (composite model system (CGO-CFO) explored "emergent" phase formation in ceramic systems as a tool to control the grain boundary composition and therefore the ionic conductivity. The segregation of Gd dopant and depletion of oxygen vacancies at the CGO-CGO grain boundary observed in single phase CGO is successfully avoided in the composites, leading to superior grain boundary ionic conductivity. This was achieved by a controlled phase reaction between the CGO and CFO phases effectively "gettering" or removing the Gd segregation at the interface into a new, emergent phase consisting primarily of Gd from the grain boundaries of CeO_2 and Fe from $CoFe_2O_4$. Local structural and chemical features of the emergent phase as a function of processing conditions and varying volume fractions of mixtures are still under investigation; however, similar emergent phases were seen
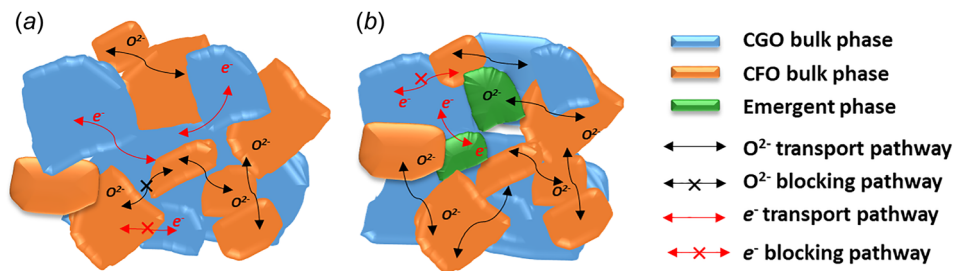

Fig. 5 CGO-CFO mixed ionic and electronic ceramic composite (a) without the formation of emergent phase and (b) with the formation of emergent phase [31]
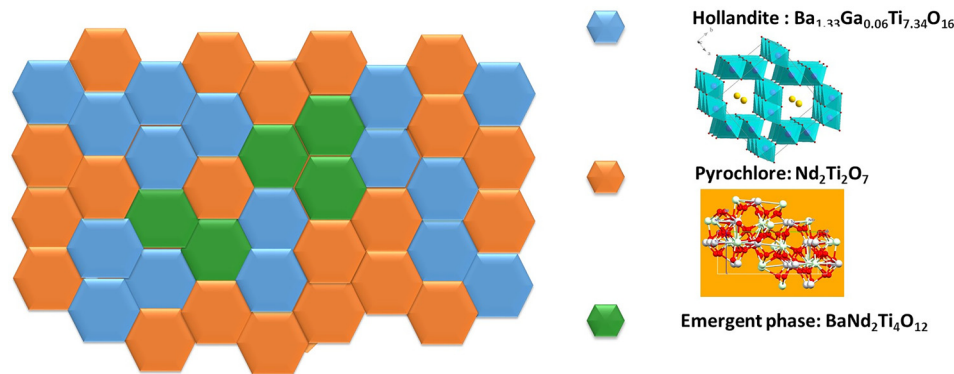
Fig. 6 Graphic depicting multiphase ceramic waste form consisting of hollandite, pyrochlore, and an emergent phase exhibiting Ba-Nd partitioning in the form $BaNd_2Ti_4O_{12}$ [75]

Legend:
Hollandite : $Ba_{1.33}Ga_{0.06}Ti_{7.34}O_{16}$
Pyrochlore: $Nd_2Ti_2O_7$
Emergent phase: $BaNd_2Ti_4O_{12}$

in a similar DP MIEC system consisting of $Ce_{0.8}Gd_{0.2}O_{2-\delta}$-$FeCo_2O_4$ (CGO-FCO) [59]. In addition to ameliorating the effects of dopant segregation at the grain boundaries for enhanced ionic transport, the emergent phase itself may participate in the ion or electronic conductive network. Figure 5 displays the (a) dual phase composite conceptually without emergent phase formation where electrons and oxygen ion transport is restricted to the relevant phase. This is contrasted with Fig. 5(b) where the emergent phase was identified as a mixed conductor and hence able to participate in both the electron and ion transport network.

Solid Electrolyte and Electrode Interface in Li-Ion Batteries. Although sufficient room temperature ionic conductivity has been achieved in solid electrolytes [61,62], significant issues remain with regards to interfacial polarization resistance to transport at the electrode/electrolyte interface, principally at the anode. The typical approach to improve the interfacial properties has been to apply thin coatings of various materials in order to reduce the polarization resistance. On anode side, ultrathin atomic layer deposition of Al_2O_3 effectively decreased the interfacial impedance from 1710 Ω cm^{-2} of the pristine Li/garnet to 1 Ω cm^{-2} of the stabilized Li/atomic layer deposition-coated garnet due to the formation of an energetically favorable Li–Al alloy at the interface that enables wetting of the metallic lithium [63].

In addition, researchers including Rupp et al. have borrowed strategies from the solid oxide fuel cell and high temperature membrane community by introducing surface microstructural modifications to address this need. A porous LLZO surface structure was infiltrated with $Li_4Ti_5O_{12}$ electrode material resulting in a ceramic/ceramic composite with demonstrated reversible cycling at low voltages [64]. Higher voltages results in the observation of emergent phases and interactions have been discovered at the LLZO/cathode interface using $LiMn_{1.5}Ni_{0.5}O_4$ LMN, with the authors raising the question of applicability of these materials systems at high voltage [65]. In fact, according to DFT calculations for the electrochemical window of LLZO, higher voltage may lead to oxidation of LLZO to Li_2O, La_2O_3, and $Li_6Zr_2O_7$ [66,67]. Other predictions and experimental results have verified these trends; for instance, $LiMn_2O_4$ (LMO) cathodes display a very high voltage around 3.6 V and has been shown to react to form secondary phases when in contact with LLZO. However, even lower voltage cathodes such as $LiFePO_4$ (LFP) have demonstrated phase reactions with LLZO. In addition, some uncertainty exists in the literature since other high voltage cathode materials $LiCoO_2$ (LCO) are expected to react, but have demonstrated appreciable phase stability with LLZO [68].

Interfacial Aspects of Multiphase Waste Forms: Hollandite and Pyrochlore. Multiphase ceramic materials that are tailored to mimic naturally occurring minerals (i.e., unique crystalline structures) that host radionuclide waste elements resulting from legacy weapons production and/or commercial nuclear fuel recycling are termed SYNROC, which is an acronym for synthetic rock, originally developed by Ringwood [53]. Assemblages of several titanate phases have been successfully demonstrated to incorporate radioactive waste elements, and the multiphase nature of these materials allows them to accommodate variation in the waste composition [69–72]. Many of the elements in the waste stream are known to react with select additives to form stable titanate based crystalline phases of the types perovskite/pyrochlore and hollandite. Elements with a +3 valance such as the most prevalent lanthanide in the waste stream, Nd^{+3}, readily form pyrochlore structures with titanium resulting in pyrochlore $A_2B_2O_7$, where A^{+3} is a lanthanide (La, Pr, Ce, Eu, Nd, Sm, Gd, Dy, Yb, and Y) [73] and B^{+4} is tetravalent titanium (i.e., $Nd_2Ti_2O_7$ type phases) [74]. The +1 valence alkali components Cs and Rb elements in the waste are known to partition to a hollandite structure. The accompanying schematic diagram depicts the multiphase assemblage that consists of SYNROC-C containing perovskite/pyrochlore and hollandite type phases (Fig. 6).

An issue that occurs during processing of the multiphase crystalline ceramic waste forms is the formation of emergent, secondary phases. For instance, Smith et al. multiple other phases such as intermetallic alloy particles, grains of calcium aluminum titanate, and titanium aluminate [76]. Formulations containing Mo waste elements often form well-known alkali molybdates such as Cs_2MoO_4 with poor aqueous durability [77]. In current SYNROC formulations targeting waste streams from potential commercial nuclear fuel recycling in the United States, the Cs containing hollandite and pyrochlore phase containing the most prevalent lanthanide Nd as $Nd_2Ti_2O_7$ constitute a majority of the phase assemblage (combined ~80%), therefore understanding interfacial interactions are of prime interest.

Emergent phase formation in these materials is driven by the overall stability of the constituent materials as a function of composition (dopant identity and concentration) as well as dopant segregation at grain boundary interfaces. In select materials combinations, a $BaNd_2Ti_5O_{14}$ phase has been observed [75] and the impact on retention of radionuclides is ongoing. Additional work is warranted on the intentional introduction of phases during processing with the aim to study how they affect isotope retention and radiation stability.

Discussion

Spatial Mapping/Imaging. The review of "emergent" phase formation in fuel cell/membrane, battery, and nuclear materials has indicated the potential for dramatic impacts on system performance. Ultimately, the overall materials properties will be determined by the 3D spatial distribution of the emergent phases

and advanced imaging techniques are required for chemical, structural, and microstructural characterization. Various imaging techniques are available for this effort, including focused ion beam-scanning electron microscopy, transmission X-ray microscopy, atom probe tomography with a wide range of spatial resolution and field of view as summarized in recent reviews [78].

At the atomic scale, atom probe tomography has recently been used to evaluate the 3D local chemistry and associated potentials in ionic conductive materials such as doped ceria, revealing the inherent complexity in grain boundary structures [79]. Recently, X-ray tomography in 3D was also utilized as input to thermodynamic to estimate spatial distribution of electrochemical fields, such as electric potential and oxygen chemical potential in MIEC materials [80]. At the mesoscale, X-ray nanotomography has been utilized to characterize the composition and 3D microstructure of the MIEC CGO oxygen ion conductive phase and a CFO electronic conductive phase, revealing the spatial distribution of the GFCCO "emergent" phases as shown in Fig. 7 [60]. Focused ion beam-scanning electron microscopy serial sectioning has become well established for 3D imaging of multiphase materials with energy applications including solid oxide fuel cell materials and can also incorporate element-sensitive imaging through the use of backscatter electron imaging or energy-dispersive X-ray spectroscopy methods [81].

Imaging has also been probed to evaluate the local composition and spatial distribution of emergent phases in nuclear material systems including hollandite [72,82]. Material system modeling that can incorporate elemental release and the interconnected microstructural network of phases to better understand the material systems' performance and degradation is also a need that needs to be addressed [83].

Thermodynamic Characterization of Emergent Phases. Throughout this article, the discussion has centered on the observation of emergent phase formation, spatial distribution, and impact on properties; however, the question of "why" they form including the details of the local thermodynamic energy landscape that favor emergent phase formation is an open question. Thermodynamic measurements such as calorimetry provide a direct measure of the energetics including formation enthalpies of resulting structures. This information is essential for the rational design of materials and prediction of their long-term performance and stability. High temperature oxide melt solution calorimetry is a versatile technique for studying the energetics of formation, solid solution mixing, phase transition, and order/disorder in ceramics making it a general tool with diverse applications in geochemistry, mineralogy, materials science, ceramics, and solid-state chemistry

[84]. The design and applications of Calvet-type heat flow calorimeter and the method of high-temperature oxide melt solution calorimetry is based on work by Navrotsky [84].

In many cases, the detailed structural features and thermodynamic properties of emergent phases such as GFCCO have not been well characterized. Calorimetery can provide standard formation enthalpies, entropies and other thermodynamic data as a function of temperature and phase transformations which allow the prediction of emergent phase formation conditions and stability of the resulting phase in composite systems [85]. For example, in Fig. 8, the known enthalpies of formation from the oxides $\Delta H_{f,ox}$ (KJ/mol) of CGO, CFO, GFO (Perovskite), and GFO (Garnet) [86–88] are plotted for comparison, revealing that the GFO (Garnet) structure is the most thermodynamically stable. However, the GFCCO emergent phase which forms in this system has a more complex set of dopant substitutions and has not yet been characterized; the position on the plot is undetermined and is symbolized by a "?." Once the formation enthalpies of emergent phases are determined, their relative stability in the multiphase assemble age can be determined from examining a number of potential reactions pathways. This approach of energy landscapes has been outlined in multiphase ceramic waste form to determine the most likely phase assemblage for hollandite and perovskite mixtures [85]. In the CGO-CFO system, one example of potential reactions can be written as

$$Gd_{0.1}FeCe_{0.4}Co_{0.3}O_{2.95} \rightarrow 0.5CoFe_2O_4 + 0.5Ce_{0.8}Gd_{0.2}O_{1.9}$$

$\Delta H_{rxn,GFCCO}$ from CFO and CGO

$$= 0.5\,\Delta H_{f,ox(CGO)} + 0.5\,\Delta H_{f,ox(CGO)} - \Delta H_{f,ox(GFCCO)}$$

Once the enthalpy of formation of GFCCO is measured, the absolute values of the reaction enthalpy $\Delta H_{rxn,GFCCO}$ can be calculated. Using this approach, Fig. 8(b) displays a plot of enthalpies of several candidate reactions of GFCCO ($\Delta H_{rxn,GFCCO}$) relative to other competing phase assemblages including GFO (P), GFO (G), CFO, and CGO. Thermodynamic data acquisition and data analysis along these lines is needed to predict emergent phase formation and stability of multiphase assemblages in ceramic composites. In fact, many emergent phases could potentially represent nonequilibrium phases that form under the specific boundary conditions of synthesis in composites or under particular operating conditions. For example, excess lithium stoichiometry in select-layered cathode materials only form under specific charging conditions V [89,90].
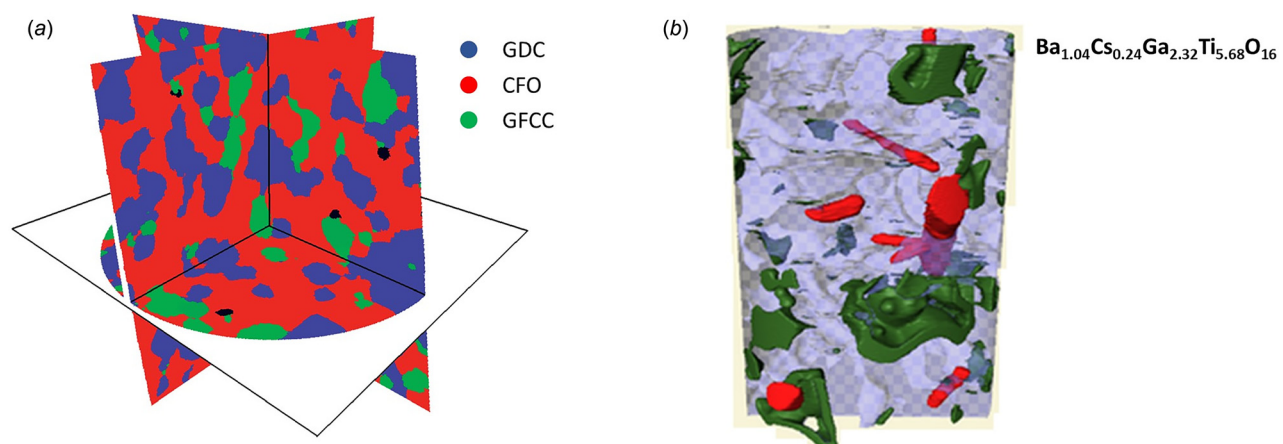

Fig. 7 (a) Orthographic revealing the 3D structure of CGO-CFO systems [60]. (Reproduced with permission from Harris et al. [60]. Copyright 2014 by Nanoscale Owner Societies) (b) 3D representation of varying Cs content observed in single-phase hollandite Ba$_{1.04}$Cs$_{0.24}$Ga$_{2.32}$Ti$_{5.68}$O$_{16}$ [82]. (Reproduced with permission from Cocco et al. [82]. Copyright by 2017 Journal of the American Ceramic Society.)
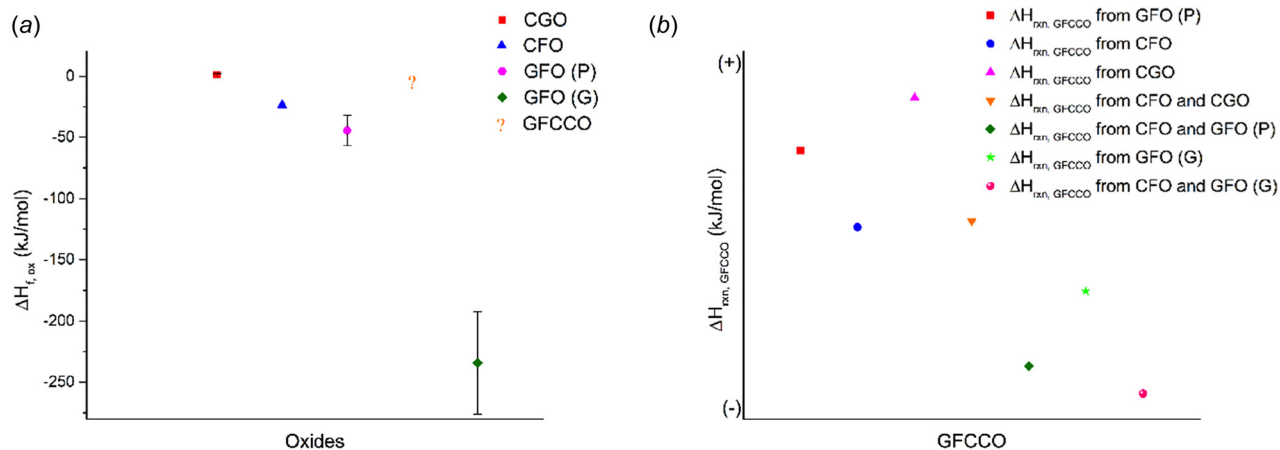
Fig. 8 (*a*) Enthalpies of formation of CGO, CFO, and GFO ($\Delta H_{\text{f,ox}}$) [86–88], and the undetermined enthalpy of formation of emergent phase GFCCO symbolized by a "?" and (*b*) enthalpies of reactions of GFCCO ($\Delta H_{\text{rxn,GFCCO}}$) relative to other competing phase assemblages including GFO, CFO, and CGO

Conclusion and Perspectives

A comparison of emergent phase formation in three application areas including solid oxide fuel cells and ionic membrane systems, solid state lithium batteries, and ceramics for nuclear waste immobilization revealed striking similarities. The behavior of model single-phase materials in these application areas including (i) CeO_2, (ii) $Li_7La_3Zr_2O_{12}$ (LLZO), and (iii) hollandite of the form $Ba_xCs_yGa_{2x+y}Ti_{8-2x-y}O_{16}$ displayed a similar behavior of grain boundary "blocking" effect toward ionic conductivity. Emergent phase formation encountered in multiphase systems applications is dictated by bulk thermodynamics, and local concentration gradients resulting from dopant segregation at interfaces. The resulting phase assemblage can either improve or impede ionic transport depending on emergent phase structure and distribution as determined by an array of potential 3D imaging techniques. Additional studies of the thermodynamic parameters, which determine the propensity for emergent phase formation, and stability of complex multiphase systems would be particularly useful. Studies at the interface between disciplines provide unique case studies for understanding materials behavior; knowledge in one application area (constrict tunnels in hollandite to immobilize cesium) can be used in other areas to enhance mobility in tunnels (enhance Li, Na, and K alkali motion in hollandite for battery applications).

References

[1] Chiang, Y. M., Lavik, I., Kosacki, I., Tuller, H. L., and Ying, J. Y., 1996, "Defect and Transport Properties of Nanocrystalline CeO2-x," Appl. Phys. Lett., **69**(2), pp. 185–187.

[2] Pergolesi, D., Fabbri, E., D'ôEpifanio, A., Di Bartolomeo, E., Tebano, A., Sanna, S., Licoccia, S., Balestrino, G., and Traversa, E., 2010, "High Proton Conduction in Grain-Boundary-Free Yttrium-Doped Barium Zirconate Films Grown by Pulsed Laser Deposition," Nat. Mater., **9**(10), pp. 846–852.

[3] Kim, Y. B., Shim, J. H., Gür, T. M., and Prinz, F. B., 2011, "Epitaxial and Polycrystalline Gadolinia-Doped Ceria Cathode Interlayers for Low Temperature Solid Oxide Fuel Cells," J. Electrochem. Soc., **158**(11), pp. B1453–B1457.

[4] Badwal, S. P. S., Deller, R., Foger, R., Ramprakash, Y., and Zhang, J. P., 1997, "Interaction Between Chromia Forming Alloy Interconnects and Air Electrode of Solid Oxide Fuel Cells," Solid State Ionics, **99**(3–4), pp. 297–310.

[5] Horita, T., Xiong, Y., Kishimoto, H., Yamaji, K., Brito, M. E., and Yokokawa, H., 2010, "Chromium Poisoning and Degradation at (La,Sr)MnO$_3$ and (La,Sr)FeO$_3$ Cathodes for Solid Oxide Fuel Cells," J. Electrochem. Soc., **157**(5), pp. B614–B620.

[6] Inaba, H., and Tagawa, H., 1996, "Ceria-Based Solid Electrolytes—Review," Solid State Ionics, **83**(1–2), pp. 1–16.

[7] Navrotsky, A., 2010, "Thermodynamics of Solid Electrolytes and Related Oxide Ceramics Based on the Fluorite Structure," J. Mater. Chem., **20**(47), pp. 10577–10587.

[8] Stefanovsky, S. V., and Yudintsev, S. V., 2016, "Titanates, Zirconates, Aluminates and Ferrites as Waste Forms for Actinide Immobilization," Russ. Chem. Rev., **85**(9), pp. 962–994.

[9] Caporuscio, F. A., Scott, B. L., Xu, H., and Feller, R. K., 2014, "Garnet Nuclear Waste Forms—Solubility at Repository Conditions," Nucl. Eng. Des., **266**, pp. 180–185.

[10] Takahashi, T., and Kuwabara, K., 1978, "Ionic Conductivities of Hollandites," Electrochim. Acta, **23**(4), pp. 375–379.

[11] Xu, Y., Wen, Y., Grote, R., Amoroso, J., Nickles, S. L., and Brinkman, K. S., 2016, "A-Site Compositional Effects in Ga-Doped Hollandite Materials of the Form $Ba_xCs_yGa_{2x+y}Ti_{8-2x-y}O_{16}$: Implications for Cs Immobilization in Crystalline Ceramic Waste Forms," Sci. Rep., **6**, p. 27412.

[12] Dillon, S. J., and Harmer, M. P., 2007, "Multiple Grain Boundary Transitions in Ceramics: A Case Study of Alumina," Acta Mater., **55**(15), pp. 5247–5254.

[13] Wang, C. M., Cargill, G. S., III, Harmer, M. P., Chan, H. M., and Cho, C. J., 1999, "Atomic Structural Environment of Grain Boundary Segregated Y and Zr

in Creep Resistant Alumina From EXAFS," Acta Mater., 47(12), pp. 3411–3422.

[14] Dillon, S. J., Tang, M., Carter, W. C., and Harmer, M. P., 2007, "Complexion: A New Concept for Kinetic Engineering in Materials Science," Acta Mater., 55(18), pp. 6208–6218.

[15] Kim, S., and Maier, J., 2004, "Partial Electronic and Ionic Conduction in Nanocrystalline Ceria: Role of Space Charge," J. Eur. Ceram. Soc., 24(6), pp. 1919–1923.

[16] Kim, S., and Maier, J., 2002, "On the Conductivity Mechanism of Nanocrystalline Ceria," J. Electrochem. Soc., 149(10), pp. J73–J83.

[17] Tuller, H. L., Litzelman, S. J., and Jung, W., 2009, "Micro-Ionics: Next Generation Power Sources," Phys. Chem. Chem. Phys., 11(17), pp. 3023–3034.

[18] Kjolseth, C., Fjeld, H., Prytz, O., Dahl, P. I., Estournès, C., Haugsrud, R., and Norby, T., 2010, "Space-Charge Theory Applied to the Grain Boundary Impedance of Proton Conducting $BaZr_{0.9}Y_{0.1}O_3$ (-) δ," Solid State Ionics, 181(5–7), pp. 268–275.

[19] Brinkman, K., Takamura, H., Tuller, H. L., and Iijima, T., 2010, "The Oxygen Permeation Properties of Nanocrystalline CeO_2 Thin Films," J. Electrochem. Soc., 157(12), pp. B1852–B1857.

[20] Bishop, S. R., Marrocchelli, D., Chatzichristodoulou, C., Perry, N. H., Mogensen, M. B., Tuller, H. L., and Wachsman, E. D., 2014, "Chemical Expansion: Implications for Electrochemical Energy Storage and Conversion Devices," Annu. Rev. Mater. Res., 44(1), pp. 205–239.

[21] Mogensen, G., and Mogensen, M., 1993, "Reduction Reactions In Doped Ceria Ceramics Studied By Dilatometry," Thermochim. Acta, 214(1), pp. 47–50.

[22] De Souza, R. A., Ramadan, A., and Horner, S., 2012, "Modifying the Barriers for Oxygen-Vacancy Migration in Fluorite-Structured CeO_2 Electrolytes Through Strain: A Computer Simulation Study," Energy Environ. Sci., 5(1), pp. 5445–5453.

[23] Yildiz, B., 2014, "'Stretching' the Energy Landscape of Oxides-Effects on Electrocatalysis and Diffusion," MRS Bull., 39(2), pp. 147–156.

[24] Shi, Y. U., Bork, A. H., Schweiger, S., and Rupp, J. L. M., 2015, "The Effect of Mechanical Twisting on Oxygen Ionic Transport in Solid-State Energy Conversion Membranes," Nat. Mater., 14(7), pp. 721–727.

[25] Kant, K. M., Esposito, V., and Pryds, N., 2012, "Strain Induced Ionic Conductivity Enhancement in Epitaxial $Ce_{0.9}Gd_{0.1}O_2$-Delta Thin Films," Appl. Phys. Lett., 100(3), p. 033105.

[26] Lei, Y. Y., Ito, Y., Browning, N. D., and Mazanec, T. J., 2002, "Segregation Effects at Grain Boundaries in Fluorite-Structured Ceramics," J. Am. Ceram. Soc., 85(9), pp. 2359–2363.

[27] Li, Z. P., Mori, T., Auchterlonie, G. J., Zou, J., and Drennan, J., 2011, "Direct Evidence of Dopant Segregation in Gd-Doped Ceria," Appl. Phys. Lett., 98(9), p. 093104.

[28] Bae, J., Lim, Y., Park, J.-S., Lee, D., Hong, S., An, J., and Kim, Y.-B., 2016, "Thermally-Induced Dopant Segregation Effects on the Space Charge Layer and Ionic Conductivity of Nanocrystalline Gadolinia-Doped Ceria," J. Electrochem. Soc., 163(8), pp. F919–F926.

[29] An, J., Bae, J., Hong, S., Koo, B., Kim, Y.-B., Gür, T. M., and Prinz, F. B., 2015, "Grain Boundary Blocking of Ionic Conductivity in Nanocrystalline Yttria-Doped Ceria Thin Films," Scr. Mater., 104, pp. 45–48.

[30] Aidhy, D. S., and Weber, W. J., 2016, "Microstructure Design for Fast Oxygen Conduction," J. Mater. Res., 31(1), pp. 2–16.

[31] Lin, Y., Fang, S., Su, D., Brinkman, K. S., and Chen, F., 2015, "Enhancing Grain Boundary Ionic Conductivity in Mixed Ionic-Electronic Conductors," Nat. Commun., 6, p. 9.

[32] Thangadurai, V., Kaack, H., and Weppner, W. J. F., 2003, "Novel Fast Lithium Ion Conduction in Garnet-Type $Li_5La_3M_2O_{12}$ (M = Nb, Ta)," J. Am. Ceram. Soc., 86(3), pp. 437–440.

[33] Murugan, R., Thangadurai, V., and Weppner, W., 2007, "Fast Lithium Ion Conduction in Garnet-Type Li(7)La(3)Zr(2)O(12)," Angew. Chem. Int. Ed. Engl., 46(41), pp. 7778–7781.

[34] Cheng, L., Park, J. S., Hou, H., Zorba, V., Chen, G., Richardson, T., Cabana, J., Russo, R., and Doeff, M., 2014, "Effect of Microstructure and Surface Impurity Segregation on the Electrical and Electrochemical Properties of Dense Al-Substituted $Li_7La_3Zr_2O_{12}$," J. Mater. Chem. A, 2(1), pp. 172–181.

[35] Huang, M. A., Liu, T., Deng, Y., Geng, H., Shen, Y., Lin, Y., and Nan, C., 2011, "Effect of Sintering Temperature on Structure and Ionic Conductivity of $Li_{7 (-) x}La_3Zr_2O_{12-0.5x}$ (x=0.5 Similar to 0.7) Ceramics," Solid State Ionics, 204–205, pp. 41–45.

[36] Awaka, J., Kijima, N., Hayakawa. H., and Akimoto, J., 2009, "Synthesis and Structure Analysis of Tetragonal $Li_7La_3Zr_2O_{12}$ With the Garnet-Related Type Structure," J. Solid State Chem., 182(8), pp. 2046–2052.

[37] Awaka, J., Akira, T., Kunimitsu, K., Norihito, K., Yasushi, I., and Junji, A., 2011, "Crystal Structure of Fast Lithium-Ion-Conducting Cubic $Li_7La_3Zr_2O_{12}$," Chem. Lett., 40(1), pp. 60–62.

[38] Jin, Y., and McGinn, P. J., 2011, "Al-Doped $Li_7La_3Zr_2O_{12}$ Synthesized by a Polymerized Complex Method," J. Power Sources, 196(20), pp. 8683–8687.

[39] Allen, J. L., Wolfenstine, J., Rangasamy, E., and Sakamoto, J., 2012, "Effect of Substitution (Ta, Al, Ga) on the Conductivity of $Li_7La_3Zr_2O_{12}$," J. Power Sources, 206, pp. 315–319.

[40] Wolfenstine, J., Sakamoto, J., and Allen, J. L., 2012, "Electron Microscopy Characterization of Hot-Pressed Al Substituted $Li_7La_3Zr_2O_{12}$," J. Mater. Sci., 47(10), pp. 4428–4431.

[41] Chen, R.-J., Huang, M., Huang, W.-Z., Shen, Y., Lin, Y.-H., and Nan, C., 2014, "Effect of Calcining and Al Doping on Structure and Conductivity of $Li_7La_3Zr_2O_{12}$," Solid State Ionics, 265, pp. 7–12.

[42] Langer, F., Glenneberg, J., Bardenhagen, I., and Kun, R., 2015, "Synthesis of Single Phase Cubic Al-Substituted $Li_7La_3Zr_2O_{12}$ by Solid State Lithiation of Mixed Hydroxides," J. Alloys Compd., 645, pp. 64–69.

[43] Kumazaki, S., Iriyama, Y., Kim, K.-H., Murugan, R., Tanabe, K., Yamamoto, K., Hirayama, T., and Ogumi, Z., 2011, "High Lithium Ion Conductive $Li_7La_3Zr_2O_{12}$ by Inclusion of Both Al and Si," Electrochem. Commun., 13(5), pp. 509–512.

[44] Wolfenstine, J., et al., 2012, "Synthesis and High Li-Ion Conductivity of Ga-Stabilized Cubic $Li_7La_3Zr_2O_{12}$," Mater. Chem. Phys., 134(2–3), pp. 571–575.

[45] El Shinawi, H., and Janek, J., 2013, "Stabilization of Cubic Lithium-Stuffed Garnets of the Type "$Li_7La_3Zr_2O_{12}$" by Addition of Gallium," J. Power Sources, 225, pp. 13–19.

[46] Li, C. L., Liu, Y., He, J., and Brinkman, K. S., 2017, "Ga-Substituted Li7La3Zr2O12: An Investigation Based on Grain Coarsening in Garnet-Type Lithium Ion Conductors," J. Alloys Compd., 695, pp. 3744–3752.

[47] Thompson, T., Wolfenstine, J., Allen, J. L., Johannes, M., Huq, A., David, I. N., and Sakamoto, J., 2014, "Tetragonal vs. Cubic Phase Stability in Al—Free Ta Doped $Li_7La_3Zr_2O_{12}$(LLZO)," J. Mater. Chem. A, 2(33), pp. 13431–13436.

[48] Liu, C., Rui, K., Shen, C., Badding, M. E., Zhang, G., and Wen, Z., 2015, "Reversible Ion Exchange and Structural Stability of Garnet-Type Nb-Doped $Li_7La_3Zr_2O_{12}$ in Water for Applications in Lithium Batteries," J. Power Sources, 282, pp. 286–293.

[49] Li, Y., Wang, Z., Cao, Y., Du, F., Chen, C., Cui, Z., and Guo, X., 2015, "W-Doped $Li_7La_3Zr_2O_{12}$ Ceramic Electrolytes for Solid State Li-Ion Batteries," Electrochim. Acta, 180, pp. 37–42.

[50] Xu, C. Y., Zhen, L., Zhang, Q., Tang, J., and Qin, L.-C., 2008, "Microstructural Characterization of Single-Crystalline Potassium Hollandite Nanowires," Mater. Charact., 59(12), pp. 1805–1808.

[51] Michiue, Y., Sato, A., and Watanabe, M., 1999, "Low-Temperature Phase of Sodium Priderite, $Na_xCr_xTi_{8-x}O_{16}$, With a Monoclinic Hollandite Structure," J. Solid State Chem., 145(1), pp. 182–185.

[52] Barbato, S., and Gautier, J. L., 2001, "Hollandite Cathodes for Lithium Ion Batteries. 2. Thermodynamic and Kinetics Studies of Lithium Insertion Into $BaMMn_7O_{16}$ (M = Mg, Mn, Fe, Ni)," Electrochim. Acta, 46(18), pp. 2767–2776.

[53] Ringwood, A. E., 1985, "Disposal of High-Level Nuclear Wastes—A Geological Perspective," Mineral. Mag., 49(351), pp. 159–176.

[54] Kesson, S. E., 1983, "The Immobilization of Cesium in Synroc Hollandite," Radioact. Waste Manage. Environ. Restor., 4(1), pp. 53–72.

[55] Carter, M. L., Gillen, A. L., Olufson, K., and Vance, E. R., 2009, "HIPed Tailored Hollandite Waste Forms for the Immobilization of Radioactive Cs and Sr," J. Am. Ceram. Soc., 92(5), pp. 1112–1117.

[56] Xu, Y., Feygenson, M., Page, K., Nickles, L. S., and Brinkman, K. S., 2016, "Structural Evolution in Hollandite Solid Solutions Across the A-Site Compositional Range From $Ba_{1.33}Ga_{2.66}Ti_{5.34}O_{16}$ to $Cs_{1.33}Ga_{1.33}Ti_{6.67}O_{16}$," J. Am. Ceram. Soc., 99(12), pp. 4100–4106.

[57] Kagomiya, I., Iijima, T., and Takamura, H., 2006, "Oxygen Permeability of Nanocrystalline $Ce_{0.8}Gd_{0.2}O_{1.9}$-$CoFe_2O_4$ Mixed-Conductive Films," J. Membr. Sci., 286(1–2), pp. 180–184.

[58] Takamura, H., Okumura, K., Koshino, Y., Kamegawa, A., and Okada, M., 2004, "Oxygen Permeation Properties of Ceria-Ferrite-Based Composites," J. Electroceram., 13(1–3), pp. 613–618.

[59] Ramasamy, M., Baumann, S., Palisaitis, J., Schulze-Küppers, F., Balaguer, M., Kim, D., Meulenberg, W. A., Mayer, J., Bhave, R., Guillon, O., and Bram, M., 2016, "Influence of Microstructure and Surface Activation of Dual-Phase Membrane $Ce_{0.8}Gd_{0.2}O_2$–$FeCo_2O_4$ on Oxygen Permeation," J. Am. Ceram. Soc., 99(1), pp. 349–355.

[60] Harris, W. M., Brinkman, K. S., Lin, Y., Su, D., Cocco, A. P., Nakajo, A., DeGostin, M. B., Chen-Wiegart, Y.-C. K., Wang, J., Chen, F., Chu, Y. S., and Chiu, W. K. S., 2014, "Characterization of 3D Interconnected Microstructural Network in Mixed Ionic and Electronic Conducting Ceramic Composites," Nanoscale, 6(9), pp. 4480–4485.

[61] Wu, J.-F., Chen, E.-Y., Yu, Y., Liu, L., Wu, Y., Pang, W. K., Peterson, V. K., and Guo, X., 2017, "Gallium-Doped $Li_7La_3Zr_2O_{12}$ Garnet-Type Electrolytes With High Lithium-Ion Conductivity," ACS Appl. Mater. Interfaces, 9(2), pp. 1542–1552.

[62] Du, F. M., Zhao, N., Li, Y., Chen, C., Liu, Z., and Guo, X., 2015, "All Solid State Lithium Batteries Based on Lamellar Garnet-Type Ceramic Electrolytes," J. Power Sources, 300, pp. 24–28.

[63] Han, X. G., Gong, Y., Fu, K. K., He, X., Hitz, G. T., Dai, J., Pearse, A., Liu, B., Wang, H., Rubloff, G., Mo, Y., Thangadurai, V., Wachsman, E. D., and Hu, L., 2017, "Negating Interfacial Impedance in Garnet-Based Solid-State Li Metal Batteries," Nat. Mater., 16(5), p. 572.

[64] van den Broek, J., Afyon, S., and Rupp, J. L. M., 2016, "Interface-Engineered All-Solid-State Li-Ion Batteries Based on Garnet-Type Fast Li+ Conductors," Adv. Energy Mater., 6(19), p. 11.

[65] Hansel, C., Afyon, S., and Rupp, J. L. M., 2016, "Investigating the All-Solid-State Batteries Based on Lithium Garnets and a High Potential Cathode—$LiMn_{1.5}Ni_{0.5}O_4$," Nanoscale, 8(43), pp. 18412–18420.

[66] Zhu, Y. Z., He, X. F., and Mo, Y. F., 2015, "Origin of Outstanding Stability in the Lithium Solid Electrolyte Materials: Insights From Thermodynamic Analyses Based on First-Principles Calculations," ACS Appl. Mater. Interfaces, 7(42), pp. 23685–23693.

[67] Han, F. D., Zhu, Y., He, X., Mo, Y., and Wang, C., 2016, "Electrochemical Stability of $Li_{10}GeP_2S_{12}$ and $Li_7La_3Zr_2O_{12}$ Solid Electrolytes," Adv. Energy Mater., 6(8), p. 9.

[68] Miara, L. J., Richards, W. D., Wang, Y. E., and Ceder, G., 2015, "First-Principles Studies on Cation Dopants and Electrolyte|Cathode Interphases for Lithium Garnets," Chem. Mater., 27(11), pp. 4040–4047.

[69] Vance, E. R., Stewart, M. W. A., and Moricca, S. A., 2014, "Progress at ANSTO on SYNROC," J. Aust. Ceram. Soc., 50(1), pp. 38–48.

[70] Amoroso, J., Marra, J., Conradson, S. D., Tang, M., and Brinkman, K., 2014, "Melt Processed Single Phase Hollandite Waste Forms for Nuclear Waste Immobilization: $Ba_{1.0}Cs_{0.3}A_{2.3}Ti_{5.7}O_{16}$; A = Cr, Fe, Al," J. Alloys Compd., 584, pp. 590–599.

[71] Amoroso, J., Marra, J. C., Tang, M., Lin, Y., Chen, F., Su, D., and Brinkman, K. S., 2014, "Melt Processed Multiphase Ceramic Waste Forms for Nuclear Waste Immobilization," J. Nucl. Mater., 454(1–3), pp. 12–21.

[72] Amoroso, J. W., Marra, J., Dandeneau, C. S., Brinkman, K., Xu, Y., Tang, M., Maio, V., Webb, S. M., and Chiu, W. K. S., 2017, "Cold Crucible Induction Melter Test for Crystalline Ceramic Waste Form Fabrication: A Feasibility Assessment," J. Nucl. Mater., 486, pp. 283–297.

[73] Brixner, L. H., 1964, "Preparation + Properties Of $Ln_2Ti_2O_7$-Type Rare Earth Titanates," Inorg. Chem., 3(7), p. 1065.

[74] Mandal, B. P., and Tyagi, A. K., 2007, "Phase Relations and High Temperature-XRD Studies of $Gd_{2-x}Nd_xTi_2O_7$ Solid Solutions," Mater. Sci. Eng. B-Solid State Mater. Adv. Technol., 136(1), pp. 46–49.

[75] Harkins, D., 2016, "The Durability of Single, Dual, and Multiphase Titanate Ceramic Waste Forms for Nuclear Waste Immobilization," M.S. thesis, Clemson University, Clemson, SC.

[76] Smith, K. L., Lumpkin, G. R., Blackford, M. G., Day, R. A., and Hart, K. P., 1992, "The Durability Of Synroc," J. Nucl. Mater., 190, pp. 287–294.

[77] Brinkman, K., Fox, K., Marra, J., Reppert, J., Crum, J., and Tang, M., 2013, "Single Phase Melt Processed Powellite (Ba,Ca)MoO4 for the Immobilization of Mo-Rich Nuclear Waste," J. Alloys Compd., 551, pp. 136–142.

[78] Cocco, A. P., Nelson, G. J., Harris, W. M., Nakajo, A., Myles, T. D., Kiss, A. M., Lombardo, J. J., and Chiu, W. K. S., 2013, "Three-Dimensional Microstructural Imaging Methods for Energy Materials," Phys. Chem. Chem. Phys., 15(39), pp. 16377–16407.

[79] Diercks, D. R., Tong, J., Zhu, H., Kee, R., Baure, G., Nino, J. C., O'Hayre, R., and Gorman, B. P., 2016, "Three-Dimensional Quantification of Composition and Electrostatic Potential at Individual Grain Boundaries in Doped Ceria," J. Mater. Chem. A, 4(14), pp. 5167–5175.

[80] Zhang, Y. X., Chen, Y., Lin, Y., Yan, M., Harris, W. M., Chiu, W. K. S., Ni, M., and Chen, F., 2016, "Electrochemical Fields Within 3D Reconstructed Microstructures of Mixed Ionic and Electronic Conducting Devices," J. Power Sources, 331, pp. 167–179.

[81] Lichtner, A. Z., Jauffrès, D., Roussel, D., Charlot, F., Martin, C. L., and Bordia, R. K., 2015, "Dispersion, Connectivity and Tortuosity of Hierarchical Porosity Composite SOFC Cathodes Prepared by Freeze-Casting," J. Eur. Ceram. Soc., 35(2), pp. 585–595.

[82] Cocco, A. P., DeGostin, M. B., Wrubel, J. A., Damian, P. J., Hong, T., Xu, Y., Liu, Y., Pianetta, P., Amoroso, J. W., Brinkman, K. S., and Chiu, W. K. S., 2017, "Three-Dimensional Mapping of Crystalline Ceramic Waste Form Materials," J. Am. Ceram. Soc., 100(8), pp. 3722–3735.

[83] Reifsnider, K., Rabbi, F., Vadlamudi, V., Raihan, R., and Brinkman, K., 2017, "Critical Path-Driven Property and Performance Transitions in Heterogeneous Microstructures," J. Mater. Sci., 52(9), pp. 4796–4809.

[84] Navrotsky, A., 2014, "Progress and New Directions in Calorimetry—A 2014 Perspective," J. Am. Ceram. Soc., 97(11), pp. 3349–3359.

[85] Xu, H., Wu, L., Zhu, J., and Navrotsky, A., 2015, "Synthesis, Characterization and Thermochemistry of Cs-, Rb- and Sr-Substituted Barium Aluminium Titanate Hollandites," J. Nucl. Mater., 459, pp. 70–76.

[86] Chen, W. Q., and Navrotsky, A., 2006, "Thermochemical Study of Trivalent-Doped Ceria Systems: CeO_2-$MO_{1.5}$ (M = La, Gd, and Y)," J. Mater. Res., 21(12), pp. 3242–3251.

[87] Reznitskii, L. A., Filippova, S. E., and Korzhukov, N. G., 1971, "Thermodynamics of the Co-Fe-O System," Russ. J. Phys. Chem., 45, pp. 529–530.

[88] Kanke, Y., and Navrotsky, A., 1998, "A Calorimetric Study of the Lanthanide Aluminum Oxides and the Lanthanide Gallium Oxides: Stability of the Perovskites and the Garnets," J. Solid State Chem., 141(2), pp. 424–436.

[89] Li, Y. Y., El Gabaly, F., Ferguson, T. R., Smith, R. B., Bartelt, N. C., Sugar, J. D., Fenton, K. R., Cogswell, D. A., Kilcoyne, A. L. D., Tyliszczak, T., Bazant, M. Z., and Chueh, W. C., 2014, "Current-Induced Transition From Particle-by-Particle to Concurrent Intercalation in Phase-Separating Battery Electrodes," Nat. Mater., 13(12), pp. 1149–1156.

[90] Yu, H. J., and Zhou, H. S., 2013, "High-Energy Cathode Materials (Li_2MnO_3-$LiMO_2$) for Lithium-Ion Batteries," J. Phys. Chem. Lett., 4(8), pp. 1268–1280.